Edge Modes as ELM Events

O.Pogutse*, J.G.Cordey, W.Kerner and B.Schunke
JET Joint Undertaking, Abingdon, Oxon., UK.
*On leave from RRC Kurchatov Institute, Moscow, Russia.

1. Introduction

The tokamak edge plasma includes a part of the core plasma and a part of the scrape-off-layer about a few Larmor radii inside and outside the separatrix. These parts have quite different topology with open and closed magnetic field lines, respectively. Due to MHD activity these two areas can interact. Therefore, this edge plasma plays a critical role in the behaviour of the entire plasma. With increasing edge temperature the dissipative instabilities in the edge plasma become weaker, the transport coefficients decrease and the gradients at the boundary increase. The profile of the pressure (along with temperature and density) becomes increasingly more step-like. For such steep gradients Larmor radius stabilisation and shear flow stabilisation take place, turbulence is suppressed and the H-mode is set up. Moreover, the development of a step-like pressure profile in the H-mode will lead to unstable MHD surface modes, which may explain the essential properties of the ELM phenomenon. The MHD instability first occurs near the X-point and gives rise to a precursor event. This instability throws out plasma from this region and destroys the separatrix in this point. Both these processes give a strong interaction with the end plates and the wall of the chamber. Due to this interaction the region near the X-point is filled by cold dirty plasma with low conductivity. This "new" plasma acts like an effective limiter for the main plasma just inside the separatrix, which becomes MHD unstable against surface modes. These surface modes have a relatively weak radial dependence which explains the macroscopic character of the ELM. This model gives an estimate for the ELM repetition time and explains, in addition, the occurrence of two different time scales during a giant ELM. The initial rise ends with a fast MHD event removing a plasma layer from the periphery. The second phase is determined by the diffusive refilling of the expelled layer.

2. Perturbed MHD equations near the separatrix. Coordinate System:

The magnetic field line geometry is described by the orthogonal coordinates ρ, ω, φ with line element $ds^2 = h_\rho^2 d\rho^2 + h_\omega^2 d\omega^2 + R^2 d\varphi^2$, where $h_\rho^2 = h_\omega^2 = \left(y_0^2 / 2^{5/2}\right) \cdot \left[1 - \cos(\omega) + \rho^2/2\right]^{-1/2}$; y_0 is the distance of the current wire from the X-point. For $\rho << 1$ this expression reduces to $h^2 = \left(y_0^2/4\right) \cdot [\omega^2 + \rho^2]^{-1/2}$. Introducing $R = R(\rho,\omega) = R_0 + x(\rho,\omega)$, where

$x(\rho,\omega) = \pm\left(y_0/\sqrt{2}\right).[-1+\cos(\omega)+\rho+\sqrt{2}(1-\cos(\omega)+\rho^2/2)^{1/2}]^{1/2}$, leads for $\rho << 1$ to $x(\rho,\omega) = \pm\left(y_0/\sqrt{2}\right)\cdot[\rho+(\omega^2+\rho^2)^{1/2}]^{1/2}$.

MHD ballooning equation:

Introducing the eikonal representation for the perturbed electrostatic potential: $\phi(t,\rho,\omega,\varphi) = \tilde{\phi}(\rho,\omega)\cdot\exp(-\gamma t + in\int_{\omega 0}^{\omega} q(\rho,\omega')d\omega' - in\varphi)$, where γ is the growth rate, leads to the ballooning stability equation:

$$\frac{1}{R}\left(\frac{B_\omega}{hB_0}\frac{\partial}{\partial\omega}\right)R\left(\frac{nq}{h}\right)^2(1+\zeta^2)\left(\frac{B_\omega}{hB_0}\frac{\partial}{\partial\omega}\right)\tilde{\phi} - \gamma^2 C_A^{-2}\left(\frac{nq}{h}\right)^2(1+\zeta^2)\tilde{\phi}$$
$$- \tilde{\phi}\frac{4\pi}{RB_0}\left(\frac{nq}{h}\right)^2\frac{1}{h^2}\left(\frac{\partial}{\partial\rho}\frac{R}{B_0} - \zeta\frac{\partial}{\partial\omega}\frac{R}{B_0}\right)\frac{dP_0}{d\rho}\tilde{\phi} = 0 \qquad (1)$$

$q = q(\rho,\omega) = \frac{B_0 h}{B_\omega R}$ denotes the safety factor and $\zeta = \zeta(\rho,\omega,\omega 0) = (\frac{\partial}{\partial\rho}\int_{\omega 0}^{\omega} q d\omega)/q$ is the shear function.

3. Stability analysis

Introducing the function $u(t)$: $\tilde{\phi}(t) = \frac{1}{\sqrt{1+t^2}}u(t)$, and expanding all quantities near the X-point leads to a Schrödinger-type equation in the new variable $t = \omega/\rho$: $u_{tt}'' + (E - V(t))u = 0$, where $E = 0$ and the "potential" $V(t)$ is: $V(t) = \left(\frac{\Gamma^2}{(1+t^2)} + \frac{1}{(1+t^2)^2} - \hat{\beta}\frac{[1+(1+t^2)^{1/2}]^{1/2}}{(1+t^2)^{3/2}}\right)$, with $\Gamma^2 = \frac{\gamma^2 q(\rho,\pi)^2 R(\pi)^2}{C_A^2}$, and $\hat{\beta} = -\frac{\sqrt{2}32\pi R(\pi)}{y_0}\frac{q(\rho,\pi)^2}{B_0(\pi)^2}\rho^{1/2}\frac{dP_0}{d\rho}$. This equation for $u(t)$ can be derived from the variational form $W = \frac{1}{2}\int_{-\infty}^{\infty}[(u_t')^2 + V(t)\cdot u^2]dt$. Choosing the trial function $u(t) = c_1$, where c_1 is constant and varying c_1 yields the condition for the growth rate $\int_{-\infty}^{\infty} V(t)dt = 0$. The resulting threshold beta (for $\gamma = 0$), is:

$$\hat{\beta}_{cr} = \int_{-\infty}^{\infty}\left(1+t^2\right)^{-2}dt \Big/ \int_{-\infty}^{\infty}\left[1+\left(1+t^2\right)^{1/2}\right]^{1/2}\Big/\left(1+t^2\right)^{3/2}dt = 0.5 \ . \qquad (2)$$

The condition for instability, $\hat{\beta} > \hat{\beta}_{cr}$, expressed through the pressure gradient near the X-point assumes the form:

$$\frac{q(\pi)^2 4\pi P_0}{B_0(\pi)^2} > \frac{y_0}{R(\pi)}\left(\frac{(\Delta x)_0}{y_0}\right)^{1/2} \propto \frac{(\Delta x)_X}{R_0}. \qquad (3)$$

We approximate $y_0 \sim b$ and $\frac{dP_0}{d\rho}$ as $\frac{P_0}{\Delta\rho} \sim \frac{P_0}{\rho}$, where $\rho \sim \Delta\rho \approx (\Delta x)_0 / y_0$; $(\Delta x)_0$ is the pressure gradient length on the separatrix in the mid-plane and $B_0(\pi)$ is the

toroidal magnetic field of the magnetic axis, $(\Delta x)_X \approx ((\Delta x)_0 y_0)^{1/2}$ is the X-point gradient length. The safety factor $q(\pi) \equiv q(\rho,\pi)$ near the separatrix is related to q by the relation $q(\rho) = q(\rho,\pi)\cdot\Lambda$, where $\Lambda = 2/\pi \ln(4\pi/\rho)$. Then it holds that $q_{95} \approx 3\cdot q(0.1,\pi)$.

4. ELM model
Nonlinear evolution:

The interchange instability occurs near the X-point. Thereby a plasma tube of width $(\Delta x)_X \approx ((\Delta x)_0 y_0)^{1/2}$ is expelled onto the target plates in the time $\tau_1 \approx [(\Delta x)_X R]^{1/2} / C_s$. The related energy loss is given by $\delta_X = \frac{\Delta W_X}{W} \approx \frac{\pi(\Delta x)_X^2}{\pi ab}\frac{P_{0edge}}{<P_0>}$, and is too small to explain the loss observed in a giant ELM. For $(\Delta x)_0 \sim 0.1$m, a ~ 1m, b ~ 1.5m and $P_{0edge}/P_0 \sim 10^{-1}$, the energy loss amounts to $\delta_X \sim 10^{-3}$, i.e. it is very small. However, the expelled plasma interacts with the target plates and as a consequence the X-point region is filled with cold dirty plasma. This plasma with low conductivity acts as a "new effective limiter". The plasma inside the separatrix now obeys unfrozen boundary conditions. It becomes unstable against a flute type instability of the main plasma with a growth rate $\tau_2 \approx [(\Delta x)_0 R]^{1/2} / C_s$. This event yields the giant ELM. Eventually a refilling of the expelled plasma inside the separatrix by hot plasma from the centre takes place on the diffusion times scale $\tau_3 \approx \tau_E(\Delta a / a)^2 \approx \tau_E / (nq)^2$ (see Figs. 1 and 3).

Scaling of the ELM frequency.
Core plasma is expelled from the region inside the separatrix with an effective radial width of the order of $\Delta a \propto a/nq$. This causes the energy loss $\Delta W \approx 2\pi ab\frac{P_{0edge}}{(nq)}$, or $\delta = \frac{\Delta W}{W} \approx \frac{2P_{0edge}}{(nq)<P_0>}$. For n ~ 1, q ~ 5 one has a loss of $\delta \approx 5\%$, which is close to typical experimentally observed values. The time to restore the lost energy by heating is given by $\frac{1}{\tau} = \frac{P}{\Delta W}$, with $W = 2\pi ab<P_0>$. Using the definition $\tau_E \approx W/P$ we can rewrite τ in the following way $\tau \approx \frac{2\pi abP_{0edge}}{(nq)P} \approx \frac{1}{nq}\frac{W}{P}\frac{P_{0edge}}{<P_0>}$. For n ~ 1, q ~ 5 and $P_{0edge}/<P_0> \sim 0.1$ this expression gives the estimate $\tau \approx 10^{-2}\tau_E \approx 1$ms. The scaling which follows from this formula for the ELM frequency is then given by:

$$f = \frac{1}{\tau} \propto nq\frac{P}{W}H_p \propto \frac{B_0 P H_p}{I^3(\Delta x)_0^{1/2}}, \qquad (4)$$

where I denotes the plasma current, P the heating power, $H_p = <P_0>/P_{0edge} \propto P_0(0)/<P_0>$ the peakness factor of the pressure profile and $(\Delta x)_0$ the mid-plane gradient length of the pressure at the separatrix (see Fig. 2).

5. Conclusions

The separatrix changes qualitatively the condition for the existence of interchange MHD instabilities. In a plasma with a separatrix the edge perturbations mainly affect the X-point. The threshold beta for the perturbations which occur just outside the separatrix is given by (3). It is found that these perturbations are more easily destablised than the corresponding internal perturbations in the closed field line region. The internal perturbations experience the stabilising effect of the magnetic well, which is absent for external perturbations. These perturbations can remove only a small fraction of the total stored energy and only destroy the magnetic separatrix near the X-point. However, these effects lead to an influx of cold and dirty plasma into the X-point region. This plasma with low conductivity acts now like an effective limiter for the plasma tube of width $\Delta a \approx a/(nq)$ inside the separatrix. It destabilises the interchange instability of the main plasma. From this scenario we can estimate the frequency of ELMs, its dependence on the plasma current, on the heating power and on the peakness factor (4). The entire process has three stages: i) appearance of the interchange instability near the X-point and filling of this region by dirty, cold plasma; ii) triggering of the major interchange instability due unfreezing and iii) refilling of the empty region inside the separatrix by hot plasma from the centre on the diffusion time scale. A reasonable correlation between the theoretical predictions and the experiment results is found.

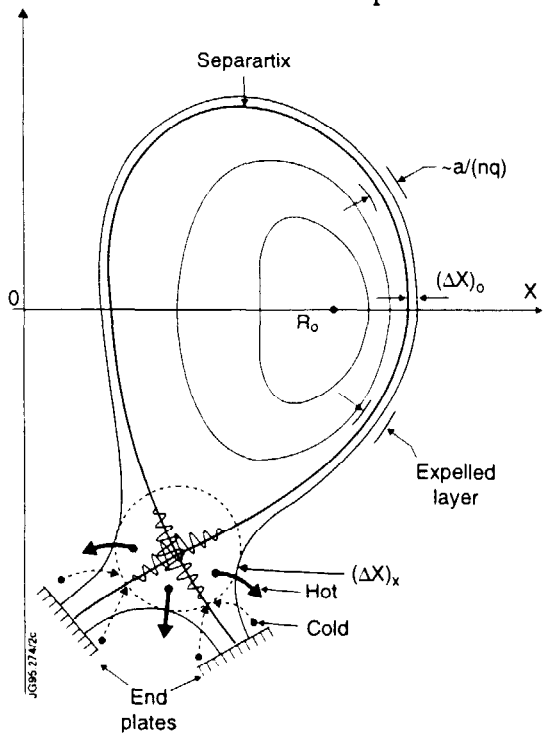

Fig. 1: Perturbations at the separatrix

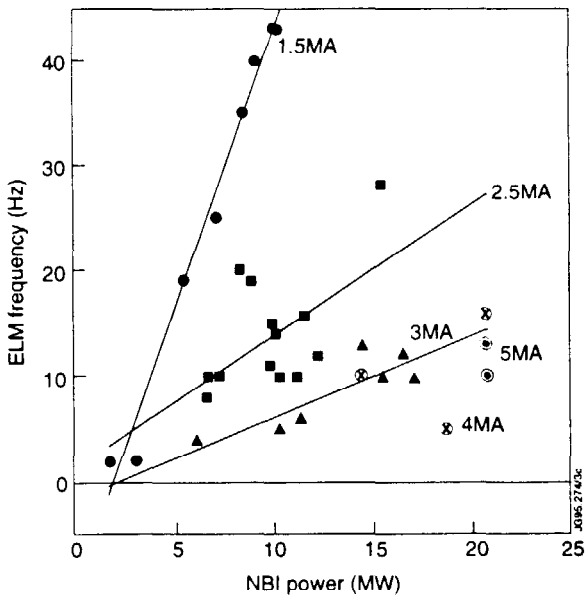

Fig. 2: ELM frequency for JET discharges

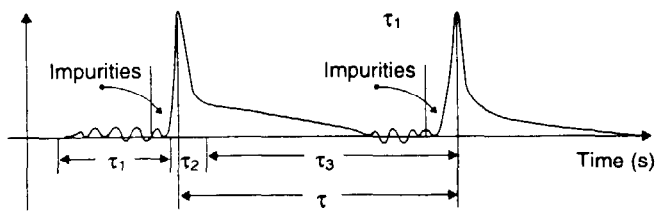

Fig. 3: Typical timescales of repetitive giant ELM's